Available online at www.sciencedirect.com
ScienceDirect
Coordination Chemistry Reviews 251 (2007) 2522–2536
COORDINATION CHEMISTRY REVIEWS
www.elsevier.com/locate/ccr

Review

Theoretical characterization of coordination space: Adsorption state and behavior of small molecules in nanochanneled metal-organic frameworks via electronic state theory, molecular mechanical and Monte Carlo simulation

Masataka Nagaoka *, Yusuke Ohta, Haruko Hitomi

Department of Complex Systems Science, Graduate School of Information Science, Nagoya University, Furo-cho, Chikusa-ku, Nagoya 464-8601, Japan

Received 23 January 2007; accepted 17 August 2007
Available online 22 August 2007

Contents

Abstract

Theoretical discussion of the coordination space created in metal-organic frameworks (MOFs), which have recently attracted many chemists, should include not only the roles of MOFs but also the characteristics of adsorbates, requiring estimates of their electronic state (ES) properties, microscopic interactions and thermodynamics of an ensemble of adsorbate molecules in dynamic responding states interacting with MOFs. This article reports, by using a combination of ES and molecular mechanical (MM) methods and Monte Carlo (MC) simulation, a sequence of theoretical chemical determination of crystal structures, adsorption energies and adsorption isobars of O_2 molecules in so-called CPL-1 (coordination polymer 1 with pillared layer structure), i.e., a MOF $[Cu_2(pzdc)_2(pyz)]_n$ (pzdc: pyrazine-2,3-dicarboxylate; pyz: pyrazine) as were synthesized recently by Kitagawa's group [R. Kitaura, S. Kitagawa, Y. Kubota, T.C. Kobayashi, K. Kindo, Y. Mita, A. Matsuo, M. Kobayashi, H.-C. Chang, T.C. Ozawa, M. Suzuki, M. Sataka, M. Takata, Science 298 (2002) 2358] and have been well-investigated by the MEM (maximum entropy method)/Rietveld method, using in situ high resolution X-ray powder diffraction data, drawing their attention on van der Waals (vdW) dimers of physisorbed O_2 locating in the middle of nanochannels (1-dim O_2 dimers ladder structure). The theoretical methods employed include molecular orbital theory, density functional theory (DFT), MM method with calibrated vdW and electrostatic parameters and grand canonical MC (GCMC) simulation.

* Corresponding author. Tel.: +81 52 789 5623; fax: +81 52 789 5623.
E-mail address: mnagaoka@is.nagoya-u.ac.jp (M. Nagaoka).
URL: http://frontier.ncube.human.nagoya-u.ac.jp/ (M. Nagaoka).

doi:10.1016/j.ccr.2007.08.016

In the DFT method, the pyrazine ring is found tilting in coinciding with O_2 adsorption and its binding energy is −10.92 kcal/mol, being in reasonable agreement with the adsorption energy at 0 K, −4.12 kcal/mol, extrapolated linearly from the calculated adsorption isobar curve by GCMC simulations, where the MM O_2 potential parameters are calibrated according to recent *ab initio* ES calculations. Finally, from the MM structural optimization, it is clearly shown that introduction of quadrupole interaction makes inclination angles of O_2 molecules dramatically in accord with the experiment results.

Keywords: Microporous metal-organic materials; Coordination space; Theoretical chemical approaches

1. Introduction

Recently, metal-organic frameworks (MOFs) [1,2] have attracted wide scientific attention owing to their unusual structures and interesting properties, with promising applications in gas separation [3], gas storage [3,4] and heterogeneous catalysis [5] as well as zeolites. Among them, a MOF, $[Cu_2(pzdc)_2(pyz)]_n$ (pzdc: pyrazine-2,3-dicarboxylate; pyz: pyrazine) which is called CPL-1 (coordination polymer 1 with pillared layer structure) [6], has been fascinating many researchers with its unique characteristics after adsorbing O_2 gas molecules. The species $[Cu_2(pzdc)_2(pyz)\cdot 2O_2]_n$, forms a one-dimensional ladder structure aligned to the host channel structure [7], where two O_2 molecules locate periodically in the middle of the nanochannels. For its further detailed understanding as coordination space under thermodynamic conditions, it is inevitable, these days, to resort to computational chemical (CC) approaches [8,9] suitable to analyze the O_2 pairing mechanism and their statistical behavior in $[Cu_2(pzdc)_2(pyz)\cdot 2O_2]_n$ satisfactorily.

In this review, we would like to introduce a combinational application of CC approaches, i.e., the electronic state (ES) calculation [10,11], the molecular mechanical (MM) treatment [12–15] and the Monte Carlo (MC) simulation [15–18], to the CPL-1 crystal adsorbing O_2 molecules, i.e., $[Cu_2(pzdc)_2(pyz)\cdot 2O_2]_n$ [7], comparing it to some other MOF systems which have been recently investigated both experimentally and also theoretically [19–21]. The first combinational CC application to gas adsorption in MOF-like materials was executed, as far as we know, by Kawakami et al. who studied the adsorption of N_2, CO_2, Ar, H_2 and O_2 on a zinc-based material, i.e., Zn(BDC) (BDC: benzene-1,4-dicarboxylate) [22] and, since then, several combinational CC studies have been reported on gas adsorption in MOFs [23–28], including the $[Cu_2(pzdc)_2(pyz)\cdot C_2H_2]_n$ system [4,29]. Only through collaboration between individually specialized CC methods, is a comprehensive understanding of the material at hand obtained.

Presently, first of all, the characteristics of CPL-1 and its O_2-adsorbd crystal $[Cu_2(pzdc)_2(pyz)\cdot 2O_2]_n$ are discussed by comparing their structures and electron density distributions obtained by the plane wave-based ES calculations, with those by X-ray powder diffraction (XRPD) experiments [7]. In particular, careful attention is paid to the importance of MOF deformation, especially the tilt of the pyrazine ring during the adsorption of O_2 molecules. This is in contrast to the $[Cu_2(pzdc)_2(pyz)\cdot C_2H_2]_n$ case where the rotational motion of an acetylene molecule itself plays also an important role in the relative stability. First, acetylene molecules are thought to be introduced into the nanochannels with their molecular axes along the nanochannel direction [4,29]. However, they can easily rotate with thermal motion in the *ac* plane within the nanochannels, and can align with one of two kinds of oxygen atoms of carboxylate bonded to a Cu ion for the first time within the restricted space of the nanochannel to form a metastable phase. Slight rotation of the pyrazine rings, and shearing of the crystal lattice in the *a* direction indicate flexible transformation for efficient guest accommodation. Subsequently, the metastable phase changes to the most stable phase with a slight rotation of acetylene molecules, and then hydrogen bonds are formed with the two uncoordinated oxygen atoms. With this change, there is now sufficient space for the pyrazine ring to rotate [4,29]. Partially, *ab initio* molecular orbital (MO) methods [11] were also used to know more precisely the molecular properties, e.g., several kinds of effective atomic point charges and the electric quadrupole (Q) moments, modeling O_2 molecules as classical rigid bodies with three interaction sites for the sake of MM and MC simulations [12–18].

Next, within the MM treatment, the O_2 molecules adsorption state in $[Cu_2(pzdc)_2(pyz)\cdot 2O_2]_n$ is optimized MM-ly by using effective vdW and electrostatic (EST) potential parameters which are recalibrated to reproduce a set of recent *ab initio* MO data [30–32] that provide us with information of the orientation and direction of O_2 molecules, especially of their pairing. For many decades, the ES and equilibrium structure of the O_2 dimer have been especially concerned with the crystal structures of solid oxygen [33–41] or the adsorption state of O_2 molecule on graphite surfaces [45–49]. Studies have explored the effective intermolecular interaction [36,37] between the two O_2 molecules and their ES description [50–54]. Further, for many years, the importance of the magnetic interaction has also been discussed [36,39–44,51–53], especially with relation to the emergence of the α-O_2 phase in solid oxygen, which is the stable state at temperatures lower than 23.9 K [34,38]. However, the β-O_2 phase was observed experimentally at temperatures higher than 43.7 K [34,38], not showing any magnetic characteristics, and the phase was also theoretically predicted to be the lowest-energy state obtained by adjusting just Lennard–Jones (LJ) parameters with the electric quadrupole–quadrupole (EQQ) interaction estimated by experimental value for the Q moment [39].

Similarly for the $[Cu_2(pzdc)_2(pyz)\cdot mO_2]_n$ system $(0 \le m \le 2)$, since the temperature involved is usually comparatively higher, i.e., typically from 70 to 300 K, it is plausible to assume that the total potential energy of an O_2 dimer could be expressed by a sum of the vdW interaction with an EQQ interaction [39]. To calibrate an analytic expression of the potential function for the O_2 dimer, both XRPD [33–36,38]

and magnetization experiments [42] and also *ab initio* ES calculations [44,50–54] are very useful and important sources of information to derive the interaction potential, as discussed elsewhere [20]. Additionally, following a number of previous studies [12–18], we determined the effective potential function for the gas-framework in the O_2-filled $[Cu_2(pzdc)_2(pyz)\cdot mO_2]_n$ system, often written as the superposition of LJ and electrostatic Coulombic potentials [20]. Then, using the MM treatments, it was shown that the present effective potential function provides us with a good theoretical basis to study the thermodynamic properties of the $[Cu_2(pzdc)_2(pyz)\cdot mO_2]_n$ system.

Finally, the O_2 molecule adsorption process should be discussed in terms of the adsorption isotherms or isobars obtained computationally by a number of grand canonical Monte Carlo (GCMC) simulations [21]. These are then compared with the experimental adsorption isotherms [7]. The *isobars* could be conveniently used for study partly because by adding pressure to a gas system this might be regarded as lowering the temperature by an appropriate amount in order to realize such a similar loading distribution of adsorbate molecules that could be "equivalently" attained under some pressure and also partly because we would like to compare the binding energy obtained by *ab initio* ES calculations with the temperature-dependent adsorption energy that is extrapolated to 0 K. Essentially, the coincidence between the computational estimate and the experimental, together with their structural similarity, should assure that the approximate expression is basically justified for the interaction potential of a light gas-absorbing MOF system. However, theoretical isotherms and isobars might be still viewed as qualified predictions since one does not always obtain good agreement between the predicted and the measured ones even now.

On the other hand, since most observables reflect chemical characteristics of the MOF system and are experimentally measured under a thermodynamic condition, e.g., a finite temperature or a finite pressure, it is inevitable that one should resort to some MC simulations which can include molecular dynamic influences or kinetic energy effects of the MOFs [55,56]. Thus, one could examine some critical behavior which might emerge under a characteristic thermodynamic condition, e.g., the tilting of pyrazine rings in $[Cu_2(pzdc)_2(pyz)\cdot 2O_2]_n$ and the emergence of metastable sorption state in $[Cu_2(pzdc)_2(pyz)\cdot C_2H_2]_n$ at 270 K under 1 kPa acetylene gas pressure [4,29]. For this purpose, not only do we need to consider the thermodynamics of adsorbate gases themselves but also the dynamic deformation of adsorbent frameworks [55–58]. The latter is actually a recent hot topic in CC treatments for water-adsorption in zeolite Na-MAP [57] and hydrated zeolite 4A [58]. The present GCMC calculation is still limited in that the framework structure must be fixed. We propose, therefore, a middle course where one might put together half in the higher temperature side of the O_2 adsorption isobar curve for an empty-CPL-1 and a lower half for the apo-CPL-1 structure of O_2-filled CPL-1. Thereby we compose a new plausible adsorption curve so as to reflect the realistic adsorbate-driven framework deformation (ADFD), i.e., the relaxation of framework distortion induced by adsorbed O_2 molecules.

2. Quantum chemical calculation

2.1. Chemical symbols for collections of copper atoms and elemental ligand molecules

For the sake of notational convenience, we would like to introduce some simplified symbols for the collections of copper atoms and elemental ligand molecules in imitation of the symbols of elements. First, a collection of two copper atoms and two pyrazine-2,3-dicarboxylate ligands, $Cu_2(pzdc)_2$, is hereafter abbreviated as Cp as a unit. Then, $[Cu_2(pzdc)_2L\cdot mH_2O]_n$ can be denoted as $[CpL\cdot mH_2O]_n$, where L is a ligand molecule, e.g., pyrazine ($m=1$) or 4,4′-bipyridine ($m=4$), etc. Further, if pyrazine and 4,4′-bipyridine are abbreviated as Py and Bp, respectively, $[Cu_2(pzdc)_2(pyz)\cdot H_2O]_n$ and $[Cu_2(pzdc)_2(bpy)\cdot 4H_2O]_n$ can be denoted concisely as $[CpPy\cdot H_2O]_n$ and $[CpBp\cdot 4H_2O]_n$ or $CpPy\cdot H_2O$ and $CpBp\cdot 4H_2O$, such as "compositional" formulae, respectively. Thus, the complex CPL-1 and CPL-2 in Kitagawa's MOF catalogue [2] can be denoted through "chemical" formulae as CpPy and CpBp, respectively.

2.2. Ab initio electronic state calculation

In the electronic state (ES) calculation of the crystal structures of $[CpPy]_n$, (i.e., CPL-1), $[CpPy\cdot 2O_2]_n$ and $[CpBp]_n$, (i.e., CPL-2), the plane wave-based density functional theory (DFT) [59–62] was applied, under periodic boundary conditions (PBCs), with the Perdew/Zunger parameterization of the Ceperley/Alder electron gas results (CA-PZ) [63,64] within the linear density approximation (LDA). Employing the ultrasoft pseudopotential (USP) method [65], the $(4\times1\times2)$ Monkhorst-Pack k-point mesh was used to sample the Brillouin zone [66], the energy cut-off was set to 300 eV, and the convergence in energy and force were 2.0×10^{-5} eV and 5.0×10^{-2} eV Å^{-1}, respectively. All the plane wave-based DFT calculations were performed using the CASTEP program package [67].

In addition, a number of *ab initio* molecular orbital (MO) calculations were carried out for small adsorbate molecules, namely, O_2, acetylene (HC≡CH) and methyl propiolate ($HC{\equiv}CHCOOCH_3$ (MP)), at the UB3LYP/6-31G(d)//UB3LYP/6-31G(d) and the B3LYP/6-31G(d)//B3LYP/6-31G(d) level of theory [68,69]. In particular, for an O_2 molecule and its dimer, additional *ab initio* MO calculations were examined at the UMP2/6-31+G(d)//UMP2/6-31+G(d) and the MP2/6-31+G(d)//MP2/6-31+G(d) level of theory [70], respectively. All these calculations used GAUSSIAN03 [71].

2.3. Characteristic structures of CpPy (CPL-1), CpPy·2O2 and CpPy·C2H2

In Fig. 1(a) and (b), shown are the optimized CpPy crystal structures without and with O_2 molecules, i.e., $CpPy\cdot 2O_2$ (monoclinic, space group $P2_1/c$ (no. 14)), respectively [6,7]. Their cell parameters are $a=4.751$ Å, $b=19.38$ Å, $c=11.31$ Å, $\alpha=\gamma=90.00^\circ$ (fixed), $\beta=99.16^\circ$, and $a=4.874$ Å, $b=20.06$ Å, $c=11.13$ Å, $\alpha=\gamma=90.00^\circ$ (fixed), $\beta=100.9^\circ$, respectively [19],

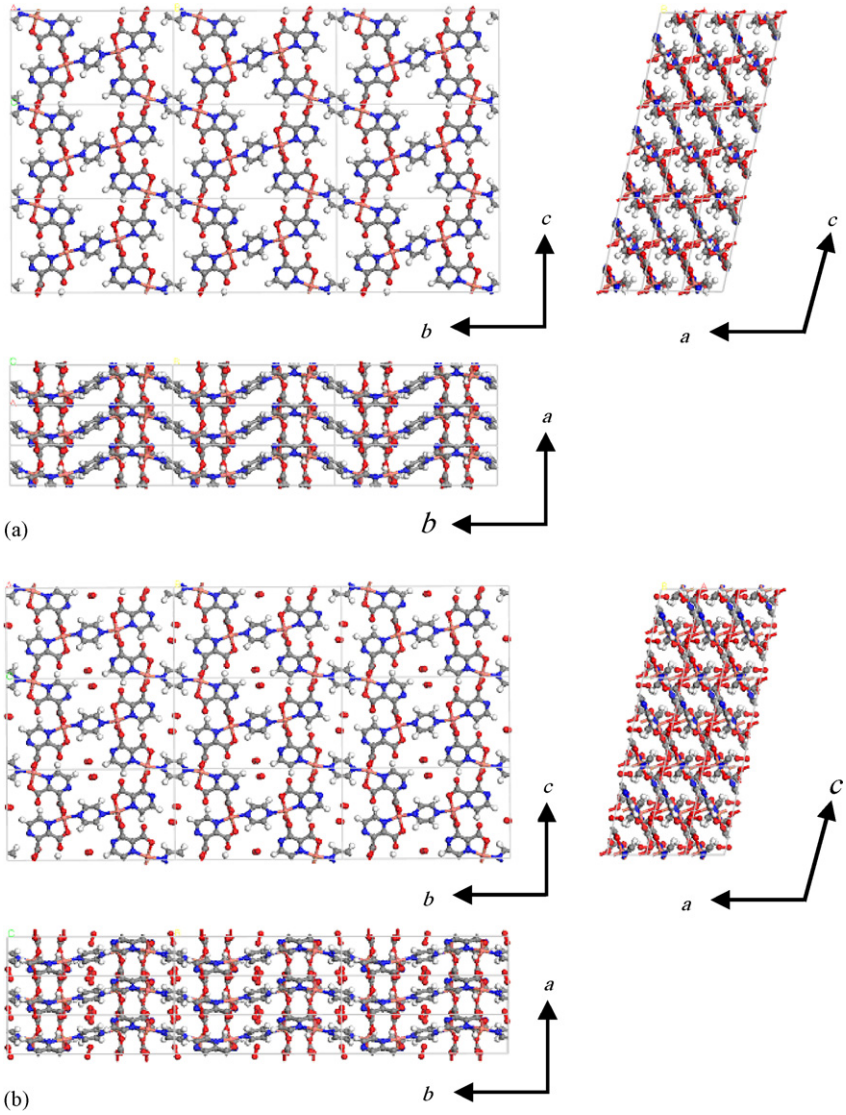

Fig. 1. Perspective views along three lattice axes of the optimized structures of CPL-1 (i.e., $[Cu_2(pzdc)_2(pyz)\cdot H_2O]_n$ or CpPy) (a) without and (b) with O_2 molecules (Cu: orange; C: gray; N: blue; H: white; O: red).

and are in satisfactorily good agreement with X-ray diffraction results; $a = 4.693$ Å, $b = 19.85$ Å, $c = 11.10$ Å, $\beta = 96.90°$ [6], and $a = 4.688$ Å, $b = 20.44$ Å, $c = 10.95$ Å, $\beta = 96.95°$ [7], respectively. For CpPy·2O_2, one can see that the experimental *b*-axis expansion is clearly reproduced and agrees with the pyrazine ring tilt explained later in Section 2.4. The adsorption saturation amount is 1.0 O_2 molecule per 1 copper atom, i.e., 2.0 O_2 molecules per 1 unit cell. That two O_2 molecules aligning parallel to each other along the *a*-axis with an inclination of about 9.50° [19] was also reproduced (cf. Table 1), in good accord with the experimental value of 11.8° [7].

Fig. 2(a) shows the total electron density (TED) and its difference at the isodensity value 0.10*e* and −0.10*e* Å^{-3}, respectively. Here, the prefix apo- means that a partial structure is taken out from the whole optimized complex structure. The TED distribution of O_2 molecules in CpPy·2O_2 (the top in Fig. 2(a)) is almost the same as that in apo-O_2 dimer (the bottom in Fig. 2(a)), showing that there is no charge transfer in CpPy·2O_2 or characteristic electron delocalization. Fig. 2(b) shows, further, the TED and its difference at the isodensity value 0.015*e* and −0.015*e* Å^{-3}, respectively, and the TED distribution of O_2 molecules in CpPy·2O_2 (the top in Fig. 2(b)) is also recognized and is almost the same as that in the apo-O_2 dimer (the bottom in Fig. 2(b)). These observations confirm there is neither charge transfer nor electron delocalization and, in this CpPy·2O_2 system, van der Waals (vdW) and electrostatic (EST) interac-

Table 1
Inclination angles of O_2 against three lattice axes of CpPy framework (angles in °)

	V_{vdW}	$V_{vdW} + V_{EQQ}$	Calculated[a]	Experimental[b]
a-Axis	24.61	11.82	9.50	11.56
b-Axis	67.19	78.36	80.72	78.48
c-Axis	87.71	94.76	102.77	97.71

[a] Numerical values were arithmetically calculated by the coordinate data obtained by the plane wave-based DFT (cf. Section 2.2).
[b] Numerical values were arithmetically calculated using the atomic coordinates reported in the XRPD experiment [7].

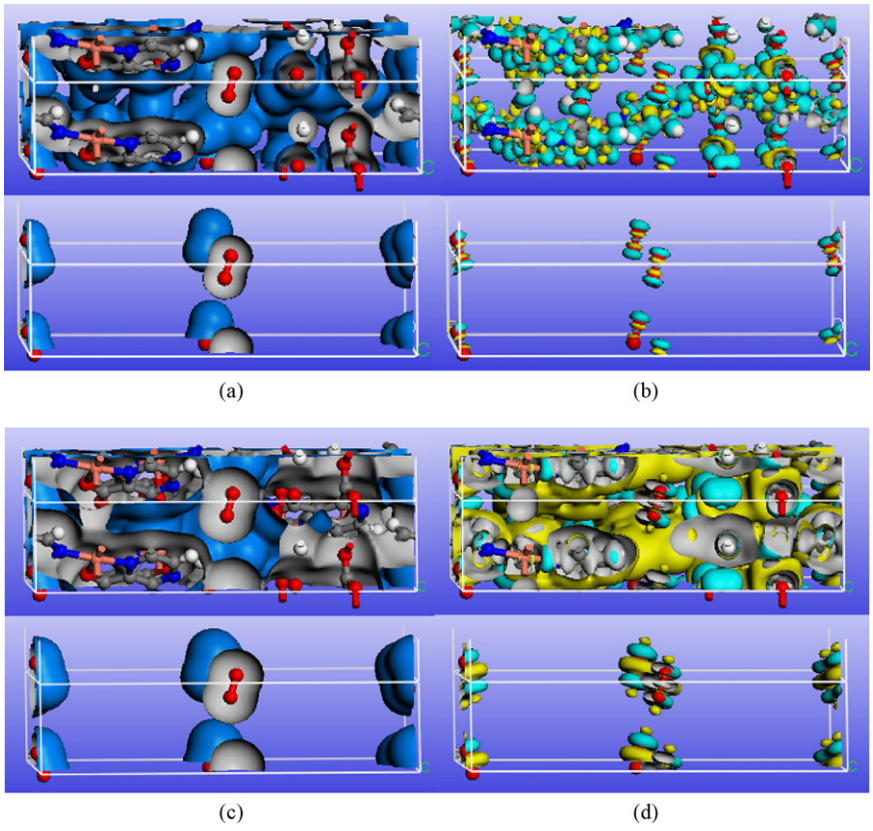

Fig. 2. Total electron densities and their differences in CpPy·2O_2 (top) and apo-O_2 dimers (bottom) (iso-value: (a) 0.10e Å^{-3} (blue), (b) 0.10e Å^{-3} (green) and −0.10e Å^{-3} (yellow), (c) 0.015e Å^{-3} (blue) and (d) 0.015e Å^{-3} (green) and −0.015e Å^{-3} (yellow)). Displayed lattice ranges are 0.00–1.48 (*a*-axis), 0.00–1.00 (*b*-axis) and 0.00–1.00 (*c*-axis).

tions are essential to stabilize the orientation between the O_2 molecules and CpPy.

In a related study, Matsuda et al. recently reported the highly controlled acetylene HC≡CH accommodation in CpPy where each end of the C_2H_2 molecule is oriented to the two non-coordinated oxygen atoms on the pore wall [4]. From the MEM/Rietveld analysis using the synchrotron XRPD data [4], it was shown that a few electrons (0.21e Å^{-3}) exist between the hydrogen atom of a C_2H_2 molecule and the free oxygen atom of the pore wall, indicating that this interaction is based not only on electrostatic attraction but also on electron delocalization between H and O atoms. In addition, the C_2H_2 molecules in the CpPy·C_2H_2 crystal, align along the *a*-axis with an inclination of 78.1° [4], whereas the pair of O_2 molecules in CpPy·2O_2 align parallel to each other along the *a*-axis with an inclination of about 11.8° [7].

One would understand from a different viewpoint later in Section 3 that the basicity of O_2 results in their tendency to reside apart from the two non-coordinated oxygen atoms of dicarboxylates on the pore wall in the nanochannel, whereas each acidic H of C_2H_2 is oriented to the two non-coordinated oxygen atoms on the pore wall.

2.4. O_2 adsorption mechanism into CpPy (CPL-1)

Fig. 3 shows concisely the O_2 adsorption mechanism into a nanochannel of the crystal structure CpPy (i.e., CPL-1), i.e., the adsorbate-driven framework deformation (ADFD). ADFD could be regarded as a 3D extension of 1D or 2D adsorbate-driven phenomena [72] which are often observed and discussed from the viewpoint of the cooperative dynamics on surfaces involving low-dimensional structural phase transition [7,72(a)] or self-assembly via dislocation reactions [72(b)]. As O_2 molecules come into the channel, the pyrazine ring tilts to accommodate them at its best orientation. This lattice transformation itself brings about energy destabilization, although the oxygen adsorption energy compensates for it, and finally leads to the stabilization as a whole. The binding energy of O_2 molecules, i.e., the adsorption energy at 0 K, was calculated from the reactant–product energy difference, between the total energy of the O_2-adsorbed CpPy, i.e., $[\text{CpPy}\cdot 2O_2]_n$ (Fig. 3(d)) and those of the empty-CpPy (Fig. 3(a)) and two free O_2 molecules. The energy balance of the CpPy systems is expressed by the following equation:

$$\Delta E_{\text{ads}} = \tfrac{1}{2}[E_{\text{CpPy}\cdot 2O_2} - (E_{\text{apo-CpPy}} + E_{\text{apo}-2O_2})] \qquad (2.1)$$

where the ES calculated energies of the anhydrous CpPy structure before adsorption ($E_{\text{apo-CpPy}}$) (Fig. 3(c)) and the O_2-adsorbed structure ($E_{\text{CpPy}\cdot 2O_2}$) (Fig. 3(d)) were estimated to be $E_{\text{apo-CpPy}} = -20843.304$ eV and $E_{\text{CpPy}\cdot 2O_2} = -24314.786$ eV, respectively. In addition, the calculated ES energy of the guest-only contribution ($E_{\text{apo}-2O_2}$) to the binding energy of the O_2 adsorbed CpPy structure was estimated to be

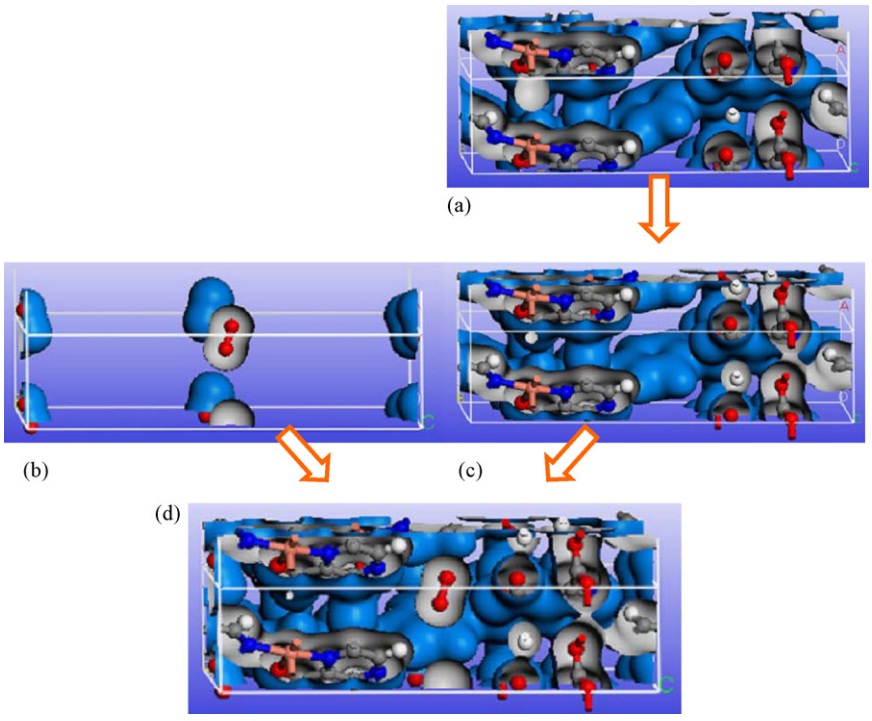

Fig. 3. O_2 adsorption mechanism into the nanopores of CpPy. Total electron densities iso-value: $0.10e$ Å^{-3} (blue) for (a) the empty CpPy framework, (b) the apo-O_2 dimer, (c) the apo-CpPy framework and (d) the CpPy·$2O_2$ complex. Displayed lattice ranges are 0.00–1.48 (*a*-axis), 0.00–1.00 (*b*-axis) and 0.00–1.00 (*c*-axis).

$E_{\text{apo}-2O_2} = -3470.534$ eV. Hence, the calculated heat of adsorption per O_2 molecule, ΔE_{ads}, showed a large negative value, −10.92 kcal/mol, indicating that the porous CpPy obtains enough stabilization energy by the adsorption of O_2 molecules, to compensate for the destabilization energy of the structural deformation, e.g., the pyrazine ring tilting. The value −10.92 kcal/mol is comparable to −9.32 kcal/mol, which was obtained as the binding energy of acetylene in the CpPy·C_2H_2 system [4,29].

3. Molecular mechanics simulation

In comparison with acetylene (C_2H_2), such small molecules as CO_2 and O_2 are adsorbed in the micropore mainly by the deep vdW potential well [4,29]. For guest molecules of this kind, we could resort to another theoretical method apart from the ES method, i.e., the molecular mechanical (MM) method [12–15], which also enables us to predict the microscopic adsorption states in nanochanneled MOFs. It is true that the *ab initio* ES method [11,67,71] is the most reliable theoretical method to predict molecular structures quantum mechanically. However, since we need to know such structure-dependent information as energy and force, concerning the interatomic interaction, the MM method is, in fact, the most convenient and realistic method for examining the thermodynamic properties or dynamic characteristics of adsorbate–framework systems such as MOFs [12–15], even if other recent methods include, e.g., the Car–Parrinello molecular dynamics (CPMD) method [16,73,74] or other *ab initio* MD methods [16,74]. Probably for the next decade, a number of molecular force fields developed to date will be useful for extensive MD calculations and MC simulations of large-scale structures.

3.1. Molecular force field

For the entire CpPy·$2O_2$ system, the total potential energy $V_{\text{CpPy}\cdot 2O_2}$ can be expressed as

$$V_{\text{CpPy}\cdot 2O_2} = V_{O_2-O_2} + V_{\text{CpPy}} + V_{\text{CpPy}-O_2} \tag{3.1}$$

where $V_{O_2-O_2}$, V_{CpPy} and $V_{\text{CpPy}-O_2}$ are the potential energies between two O_2 molecules, within CpPy, and between O_2 and CpPy, respectively (e.g., [47(b)]). As stated previously, in the CpPy·$2O_2$ system, the adsorbate–framework interaction $V_{\text{CpPy}-O_2}$ should consist mainly of the deep vdW potential [4,7]. Actually, as shown in Figs. 1 and 4(a), the oxygen molecule in a nanopore of the nanochannel in CpPy is enclosed almost equally with six hydrogen atoms of the surrounding pyrazine rings, their interatomic distances ranging from 2.744 to 3.441 Å (Fig. 4(a)). In the CpPy·C_2H_2 system, the C_2H_2 molecule has a clear linear form with acidic hydrogen atoms at both ends toward the two non-coordinated oxygen atoms on the pore wall [4,29]. However, the preparation of $V_{O_2-O_2}$ must be made carefully because one O_2 molecule in CpPy·$2O_2$ interacts not only with the pore surface atoms but also other O_2 molecules in the one-dimensional ladder structure along the host nanochannel with two typical interatomic distances 3.203 and 3.483 Å (Fig. 4(b)). Appendix A provides a brief explanation on molecular solids and the vdW dimers, and explains rather precisely how these theoretical analyses can be used to construct the intermolecular potential parameters of the present O_2 dimer system. Molecu-

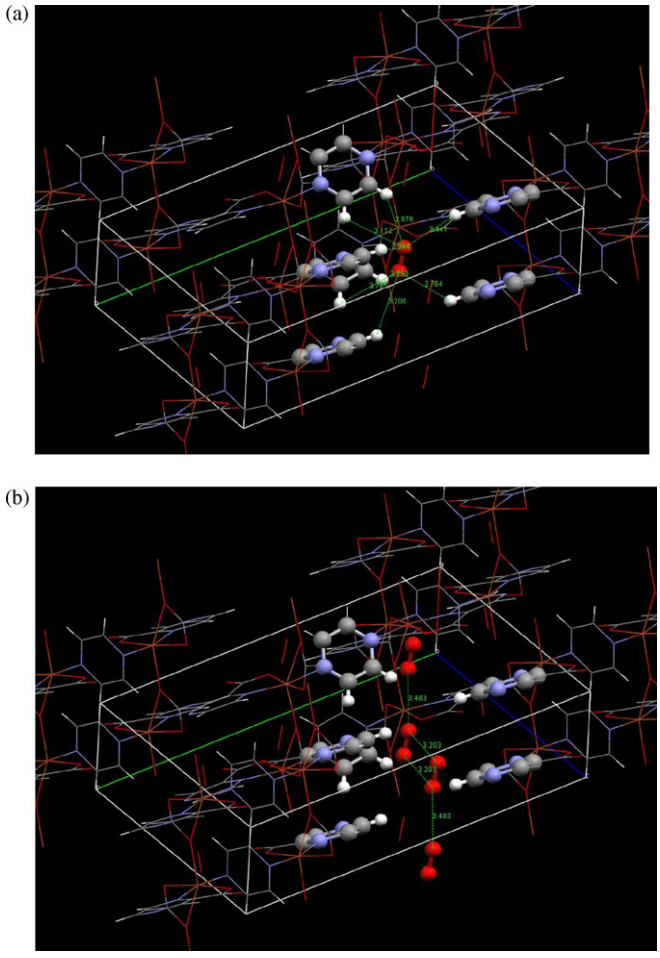

Fig. 4. (a) The adsorbate–framework interaction and (b) the adsorbate–adsorbate interaction.

lar force field parameters are also provided for other constituent atoms in the CpPy·$2O_2$ system.

3.2. Molecular-mechanically optimized CpPy·$2O_2$ structure

The position and orientation of O_2 molecules were optimized to minimize their MM interaction energy $V_{CpPy\cdot 2O_2}$ (Eq. (3.1)). The CpPy framework was fixed to that of apo-CpPy in the CpPy·$2O_2$ structure obtained in the XRPD experiment. While the O_2 molecules were treated as rigid bodies, a structural constraint was applied to the periodic framework CpPy model by fixing not only the unit cell parameters but also all the atomic positions to those of the apo-CpPy structure [20]. The convergence criteria were assumed to be 0.100 kcal/(mol Å) for the RMS atomic force, 1.000×10^{-3} kcal/mol for the overall energy difference and 3.000×10^{-3} Å for the RMS overall displacement [75].

In Fig. 5(a) and (b), the MM-optimized structures of CpPy·$2O_2$ are shown from the c-axis, using only the vdW interaction (V_{vdW}) and the vdW and EQQ interaction ($V_{vdW} + V_{EQQ}$), respectively. It is clearly recognized that the effective potential $V_{vdW} + V_{EQQ}$ optimized after introducing the V_{EQQ} interaction,

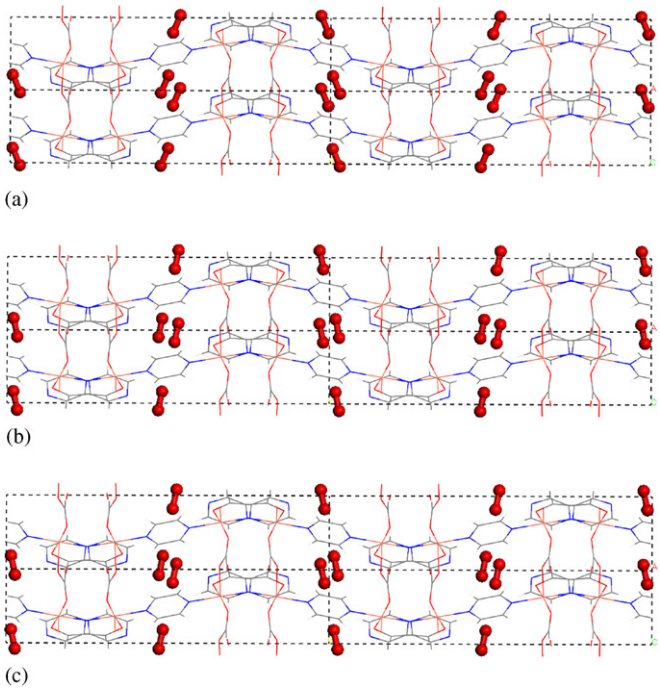

Fig. 5. Optimized CpPy·$2O_2$ structure with (a) V_{vdW} and (b) $V_{vdW} + V_{EQQ}$, and (c) XRPD structure (80 kPa/O_2 gas, 90 K).

should improve the O_2 inclination angle to be coincident with that in the experiment (Fig. 5(c)) [7]. This is slightly different from the angle obtained by optimizing with only the V_{vdW} interaction (Fig. 5(b)). In Table 1, in order to show this remarkable coincidence more clearly, we present the numerical values of inclination angles of O_2 against three lattice axes of the CpPy framework and show that the inclusion of the V_{EQQ} interaction dramatically improves them. It is concluded, therefore, that the inclusion of the EQQ interaction to O_2 is quite important and essential to reproduce its orientation in CpPy.

A number of recent references note the importance of including the electrostatic potential for homonuclear diatomic molecules, e.g., H_2 [23–25,76]. Indeed, nearly two decades ago, there was such a report that the $0.11D$ dipole moment of carbon monoxide does not contribute significantly to its rotational motion in myoglobin, which is determined almost entirely by the electric Q moment [77]. In fact, it was found that the dipole moment must be increased by a factor of 10 to mimic the correlation resulting from the Q moment [78].

3.3. Methyl propiolate incorporated in the nanochannel of CpBp (CPL-2)

In comparison with CPL-1 (i.e., CpPy in the present notation of "chemical" formula), let us consider here CPL-2 (i.e., CpBp), the second entry in Kitagawa's MOF catalogue of CPLs [2,6]. In Fig. 6, shown are the optimized CpBp crystal structure (monoclinic, space group $P2_1/c$ (no. 14)). The cell parameters are $a = 4.849$ Å, $b = 27.64$ Å, $c = 11.60$ Å, $\alpha = \gamma = 90°$ (fixed), $\beta = 102.5°$, respectively, and are found in satisfactorily good agreement with those XRPD results; $a = 4.764$ Å, $b = 27.97$ Å, $c = 10.90$ Å, $\alpha = \gamma = 90.0°$, $\beta = 96.51°$, respectively

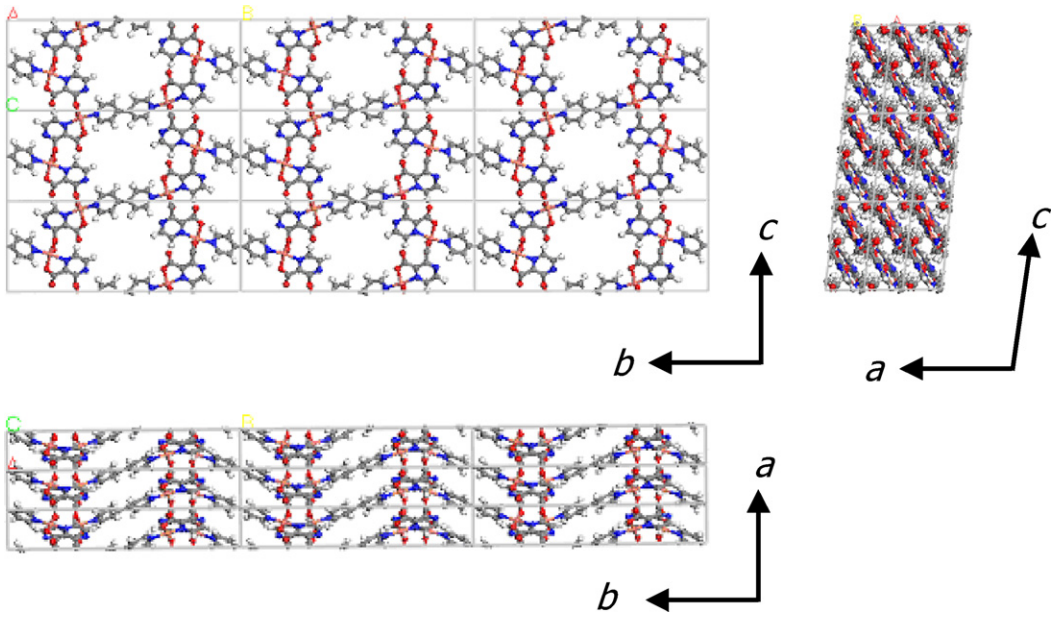

Fig. 6. Perspective views along three lattice axes of the optimized structure of CPL-2 (i.e., $[Cu_2(pzdc)_2(bpy)]_n$ or CpBp) (Cu: orange; C: gray; N: blue; H: white; O: red).

[2,6]. Although CpBp has a pore size 8.2 Å × 6.0 Å, larger than CpPy (4.0 Å × 6.0 Å) (Fig. 1), it is narrow enough for a specific chemical reaction to proceed. For example, Uemura et al. reported the first radical polymerization of styrene in CpBp, providing stable propagating radicals (living radicals); a specific space effect of the host frameworks on the monomer reactivity is demonstrated [79].

Further, in the synthesis of poly(substituted acetylenes), the nanochannel structure would direct the selectivity towards a polymerization with *trans* addition because of the prohibitive steric demand for the formation of trisubstituted benzenes and *cis* polymers [80]. As shown in Fig. 7(a), methyl propiolate (MP) $HC{\equiv}CCOOCH_3$ is a monosubstituted acetylene which bears an electron-withdrawing substitution group $–COOCH_3$ and shows

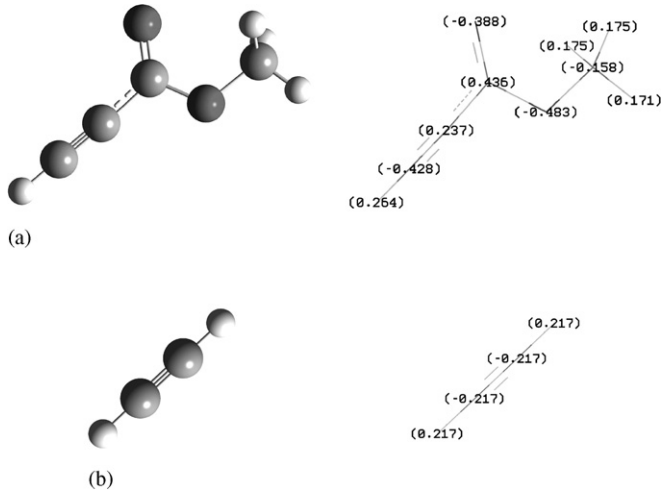

Fig. 7. Structures and atomic charges of (a) methyl propiolate and (b) acetylene from the electronic state calculation (B3LYP/6-31G(d)//B3LYP/6-31G(d)) (C: gray; O: red; H: white).

more acidic characteristic than acetylene itself (Fig. 7(b)). This is clearly reproduced by the ES calculation even at the B3LYP/6-31G(d)//B3LYP/6-31G(d) level of theory: The partial atomic point charge on the terminal hydrogen is 0.264*e* in MP (Fig. 7(a)), while that in acetylene is 0.217*e* (Fig. 7(b)).

In both CpPy and CpBp, there exist basic surface oxygen atoms that act as specific adsorption sites for guest molecules and fix strongly acidic hydrogen atoms to them (cf. Fig. 6). CpPy has a pore size (4.0 Å × 6.0 Å) suitable to accept an acetylene molecule tightly bound at each end to the non-coordinated carboxylate oxygen atoms. On the other hand, since CpBp has a larger pore (8.2 Å × 6.0 Å) than CpPy, abstraction of one proton per acetylene molecule might occur at the Lewis basic sites on the pore wall and might produce reactive acetylide species by C–H bond dissociation, which subsequently initiate anionic polymerization [79].

In addition, as shown in Fig. 8(a), the MM-optimized structure, using the universal force field (UFF), reproduces a specific hydrogen-bonding interaction between an MP monomer and two oxygen atoms in the carboxylate moiety in CpBp (Fig. 8(a)). The $–C{\equiv}CH$ group of MP is clearly oriented towards the carboxylate oxygen atoms on the pore wall, and the acetylenic hydrogen atom and the oxygen atoms are close enough for efficient hydrogen bonding (2.8 and 2.9 Å), which is consistent with the experimental results. In Fig. 8(b), a schematic illustration is shown for randomly aligned MP molecules in the nanochannel in CpBp, which are found closely packed in fact for controlling the stereostructure (the *cis* and *trans* chain sequence) [80].

4. Grand canonical Monte Carlo simulation

To derive the thermodynamic properties of an ensemble of adsorbate molecules in a MOF structure, we execute the grand

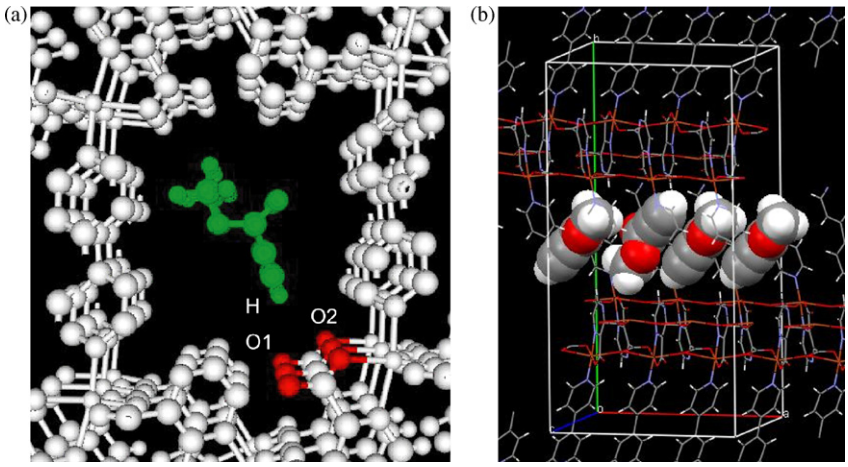

Fig. 8. (a) MM-optimized structure of one MP incorporated in the nanochannel. The distances between a hydrogen atom of MP and two oxygen atoms of the pzdc ligand in the host are 2.9 Å (H–O1) and 2.8 Å (H–O2). Hydrogen atoms of the host was omitted for clarity. The guest MP and the interacted oxygen atoms are colored with green and red, respectively. (b) Schematic illustration for randomly aligned MP molecules in the nanochannel in CpBp (C: gray; O: red; H: white).

canonical Monte Carlo (GCMC) simulations [15–17] according to the computational scheme explained in Appendix B.

4.1. Average loading distribution of O_2 in CpPy at 90 K under 80 kPa O_2 gas pressure

Fig. 9 shows the average loading distribution of O_2 in CpPy at 90 K under 80 kPa O_2 gas pressure, which was obtained through the GCMC simulation of the mass cloud distribution of all the adsorbed O_2 molecules [21]. In XRPD results, the peanut-shaped electron densities, which are believed due to O_2 molecules, were clearly recognized in the middle of the channels [7], while a similar distribution is observed in Fig. 9 as a pair of green peanut-shapes per pore. Although their shapes seem to be relatively little longer (cf. the bottom left in Fig. 9) in comparison to those of MM-optimized O_2 molecules (Fig. 5(b)), this is probably a temperature effect. The stable binding O_2 pair per unit cell corresponds clearly to the same saturated amount of adsorption of 1.0 O_2 molecules per copper atom reported experimentally under the same thermodynamic conditions [7].

In Fig. 10, plotted are adsorption isobars of the average number (deep blue curve) and the average adsorption energy (red curve) of adsorbed O_2 molecules per unit cell in the temperature range from 70 to 200 K under 80 kPa O_2 gas pressure. One can find reasonably that the average number increases as the temperature decreases. However, the critical temperature that O_2 molecules start to enter into the nanopores, is higher in the apo-CpPy (Fig. 10(b)) than that in the empty-CpPy (Fig. 10(a)). This is because the apo-CpPy is maintained as an ideal structure which could be most advantageous to accept O_2 molecules (Fig. 3(c)). On the contrary, the original empty-CpPy should take the most stable structure by itself in the absence of O_2 molecules (Fig. 3(a)). Thus, what should really occur to the framework structure must be a sudden change, occurring simultaneously

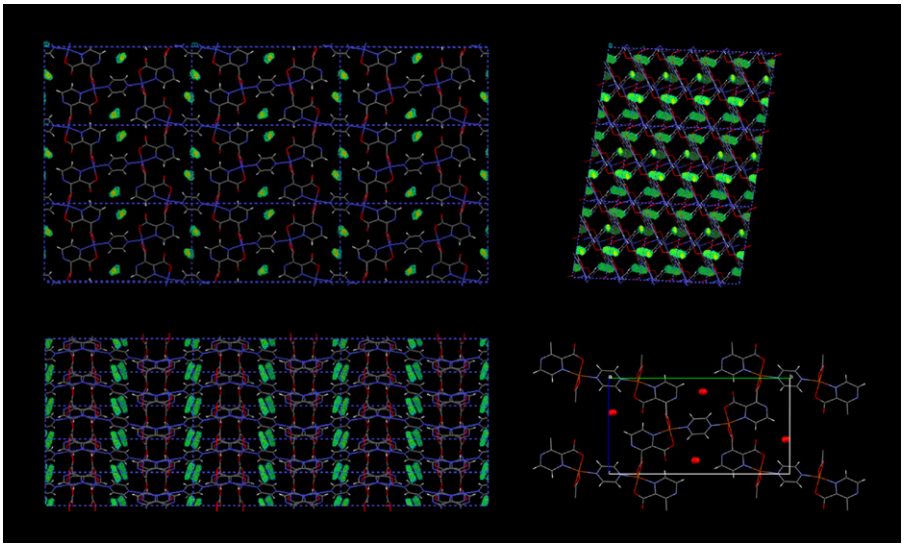

Fig. 9. Average loading distribution of O_2 in CpPy at 90 K under the O_2 gas pressure 80 kPa; perspective views along *a*-axis (top left), along *b*-axis (top right), along *c*-axis (bottom left) and the experimental crystal structure along *a*-axis (bottom right) for comparison. Green clouds indicate the existence regions of adsorbed O_2 molecules.

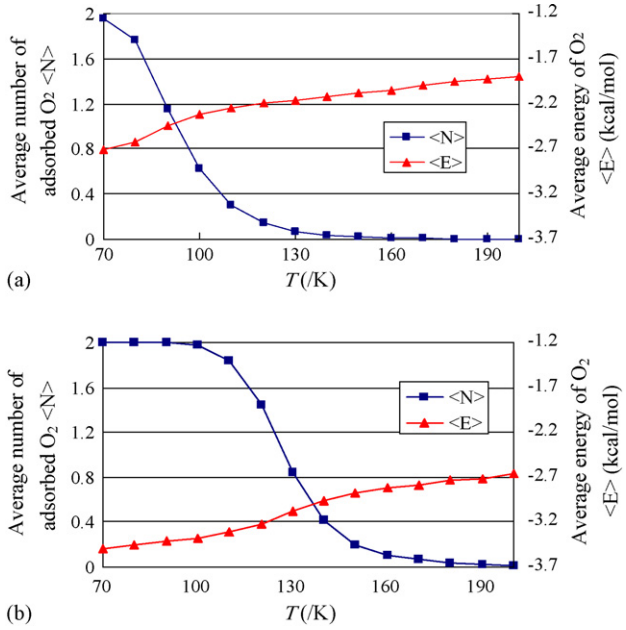

Fig. 10. Average number of adsorbed O_2 molecules per unit cell (deep blue curve) and average adsorption energy per unit cell (red curve) for (a) the empty-CpPy and (b) apo-CpPy framework structure.

with absorbing O_2 molecules, from the empty structure to the apo-structure, i.e., the adsorbate-driven framework deformation (ADFD) [72]. We will consider this perspective in the following subsection.

4.2. Framework relaxation influence on O_2 adsorption and average adsorption energy

It was experimentally observed that the O_2 adsorption suddenly occurs around 130 K [7]. However, from both GCMC simulations using the empty- or the apo-CpPy framework, it occurs rather gradually in each simulation and the isobar curve does not provide us with a good estimate of the gate temperature at which the adsorption process should start (Fig. 10(a) and (b)). This is because the present GCMC calculation has a limitation that the framework structure must be fixed. Thus, presuming that the real framework deformation suddenly occurs triggered by some pump-priming adsorbate molecules, we have synthesized realistic composite curves (solid curves in Fig. 11) from the two half curves, i.e., the higher-temperature half in Fig. 10(a) and the lower one in Fig. 10(b), so as to reflect approximately the real ADFD, i.e., the relaxation of framework distortion induced by adsorbed O_2 molecules (Fig. 3).

With the aid of these curves, as shown in Fig. 11, it can be anticipated that the average number of O_2 molecules would increase suddenly from 0.0 to 2.0 and the average adsorption energy would decrease from −2.2 to −3.3 kcal/mol through a narrow temperature range between 110 and 120 K. This corresponds reasonably to the experimental evidence that, in the susceptibility χ of CpPy with O_2, the contribution $\Delta\chi$ from adsorbed O_2 molecules similarly increases by 0.15×10^{-2} to 1.3×10^{-2} emu/mol with decreasing temperature in almost the same range, and, in synchrotron XRPD pattern, there seems to be a discontinuity between 130 and 150 K [7]. On the other hand, the average energy of O_2 decreases from −1.95 to −3.45 kcal/mol with temperature decrease through a sudden decline around 115 K. From the fact that an appropriate inclusion of the electric quadrupole–quadrupole (EQQ) interaction of O_2 in addition to the vdW interaction, has improved the O_2 saturation temperature by 30 K (not shown explicitly in this review [21]), the adsorption isobar would benefit from further tuning of the molecular force field parameters [12,90] and would agree much better with the experimental one by taking also the framework parameters into account.

Fig. 12 shows a prediction line (thick black one) of the average adsorption energy $E_{ads}(T)$ of the O_2 molecule in the lower temperature range, linearly extrapolating the original curve (red wavy curve) obtained by GCMC simulations of O_2 molecules for apo-CpPy framework (Fig. 10(b)). If E_{ads} were expressed as a linear function of T:

$$E_{ads}(T) = AT + E_{ads}(0) \tag{4.1}$$

where A and $E_{ads}(0)$ are the slope and the intersect along the $\langle E \rangle$ axis, respectively, the adsorption energy at 0 K, i.e., $E_{ads}(0)$, would become simply −4.12 kcal/mol, the slope A being estimated as 0.00728 kcal/(mol K). In Section 2.4, we have shown an evaluated binding energy of O_2 molecule ΔE_{ads} as −10.9 kcal/mol by *ab initio* ES calculations and, since ΔE_{ads} should correspond to $E_{ads}(0)$, the value −4.12 kcal/mol by the GCMC calculation is considered in reasonably good agreement with −10.9 kcal/mol.

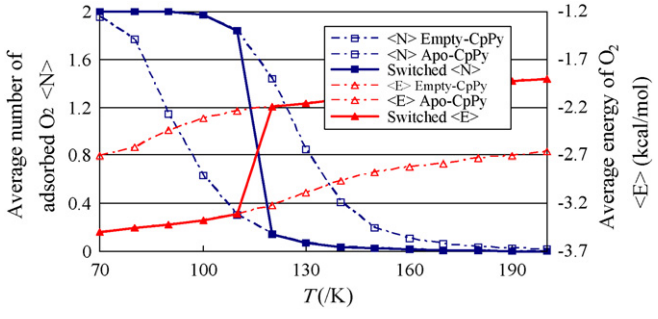

Fig. 11. Composite curves obtained by putting together two curves of the average number and the average adsorption energy of O_2 molecules in apo-CpPy (CpPy-2O_2) and the empty CpPy structures.

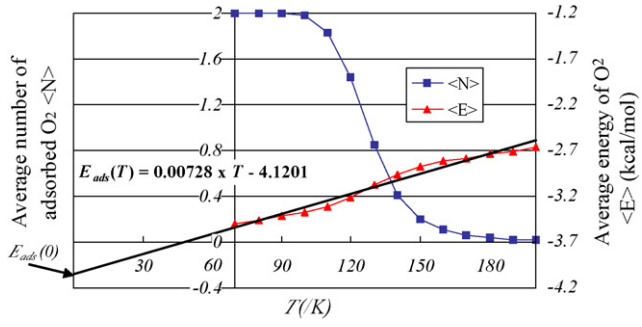

Fig. 12. Average adsorption energy of O_2 molecule extrapolated linearly to 0 K from those by the GCMC simulation for apo-CpPy framework.

In comparison to acetylene molecules, e.g., those in $CpPy{\cdot}C_2H_2$ [4,29], since oxygen should be adsorbed physically rather than chemically, it might be expected that the adsorption energy per O_2 molecule should be a little smaller than that of acetylene, i.e., −9.32 kcal/mol [4]. However, it is also true that, in the $CpPy{\cdot}2O_2$ system, not only the vdW potential-energy will give birth to by the CpPy framework and the other O_2 molecule but also the EST interaction originating from the O_2 electric Q moment, should be very influential in the energy stabilization. In any case, one needs at present more extensive *ab initio* ES calculations to deduce the final conclusion at the level of chemical accuracy, examining both the validity of theoretical approximations adopted and the numerical accuracy of computation.

5. Conclusions

Describing theoretically or computationally the structures and dynamics of MOFs is still a challenging task even today when the most recent computer technology allows the multi-scale simulation for multi-chemistry of small-to-middle size molecules. However, to attack such typical phenomena in modern coordination chemistry regarding MOFs, e.g., gas adsorption in MOFs and chemical reactions occurring in their nanospaces, some combinational computational chemical (CC) approaches, i.e., the electronic state (ES) calculation, the molecular mechanical (MM) treatment and the Monte Carlo (MC) simulation, are powerful and realistic strategies these days. The present situation of CC approaches to MOFs is quite similar to that to such microscopic interior structures at the active sites of proteins, where catalytic or photochemical reactions take place, e.g., O_2 adsorption and desorption processes in myoglobin [77,81].

In this review, taking the nanochannel of CPL-1, i.e., $[Cu_2(pzdc)_2(pyz)]_n$ as a characteristic example among those nanospaces that MOFs produce, we reported some recent results using combinational CC approach. First, the optimized CPL-1 crystal structures without and with O_2 molecules, (i.e., $[Cu_2(pzdc)_2(pyz)]_n$ and $[Cu_2(pzdc)_2(pyz){\cdot}2O_2]_n$, respectively), obtained by the plane wave-based density functional theory (DFT) [19], were introduced with their cell parameters which were in satisfactorily good agreement with experimental X-ray powder diffraction (XRPD) experiments [7]. The alignment of the two O_2 molecules parallel to each other along the *a*-axis with an inclination of ca. 9.50° was in good accord with the experimental value 11.8° (or 11.52°). Second, the MM parameters for the O_2 dimer were optimized including appropriately the electrostatic interaction between O_2 molecules as the electric quadrupole–quadrupole (EQQ) interaction. From the MM structural optimization, the introduction of the EQQ interaction provides inclination angles of the O_2 molecules in exceptionally good accord with the experimental data, e.g., 11.82° versus 11.56° for the *a*-axis (Table 1). Third, the average adsorption energy per O_2 at 0 K, was −4.12 kcal/mol by extrapolating the grand canonical Monte Carlo (GCMC) results, corresponding reasonably to the *ab initio* ES calculation (−10.92 kcal/mol). From the fact that from these MM parameters we can derive very well the O_2 saturation temperature in the adsorption isobar curves in the GCMC results, together with the excellent agreement in the inclination angle, we conclude that, for adsorption phenomena in MOFs, at least in CPL-1, even such a neutral gas molecule without a electric dipole moment, should be dealt with by including the electrostatic interaction, i.e., the EQQ interaction in O_2 molecules. This observation is completely consistent with the recent observation by Garberoglio et al. that the effect of electrostatic potential on hydrogen adsorption in MOFs is very significant at low coverage [25] and mutually compatible with the opinion by Yang and Zhong that even the atomic partial charges of the framework should be taken into account [27,28].

At present, most of all GCMC simulations of gas molecule adsorption in MOF systems have a limitation that their framework structures must be fixed. However, on account of the adsorbate-driven framework deformation (ADFD), the lattice dynamics of the MOF must be taken into account during gas molecule adsorption [55–58]. Because ADFD could be regarded as a 3D extension of 1D or 2D adsorbate-driven phenomena [72] which have been often observed and discussed from the viewpoint of the cooperative dynamics on surfaces involving low-dimensional structural phase transition [7,72(a)] or self-assembly via dislocation reactions [72(b)], analogous studies of MOFs relevant to ADFD must be developed in future, turning to advantage the previous accomplishments in the field of zeolites and related materials [82]. Furthermore, since the nuclear quantum effect is also important for hydrogen adsorption at low temperature, some realistic prescription applicable to multi-scale phenomena with huge degrees of freedom must be established immediately, e.g., the development of the quadratic Feynman–Hibbs (FH) effective potential [28,76(b),83].

Finally, we would like to note that now is the most appropriate and the best time to theoretically characterize those pores and their walls in nanochannels formed in a number of MOFs. It will become very important and significant in the near future to study them together with their dynamics, e.g., diffusion process [84,85] and chemical reactions [79,80], reflecting that coordination space on the basis of MOFs might open up new and innovative industrial applications in gas storage, separation and heterogeneous catalysis, etc.

Acknowledgements

The authors' work discussed in this article was carried out with Profs. Susumu Kitagawa, Takashi Uemura (Kyoto University), Ryotaro Matsuda (Kyushu University) with help from Prof. Ryo Kitaura (Nagoya University). Drs. Masaki Takata (JASRI/Spring-8), Yoshiki Kubota (Osaka Prefecture University) and Tatsuo C. Kobayashi (Okayama University) are acknowledged for the discussion of crystal structures of CPL-1 and its small molecule-adsorbed complexes. MN is also grateful to Prof. Masaki Kawano for his informative discussion in the early stage of the present research. This work was mainly supported by a Grants-in-Aid for Scientific Research in a Priority Area "Chemistry of Coordination Space" (#434) from the Ministry of Education, Culture, Sports, Science and Technology in Japan and partially by a Grant-in-Aid for the 21st Century COE (Centers of Excellence) program "Frontiers

of Computational Science" at Nagoya University, and also by the Core Research for Evolutional Science and Technology (CREST) "High Performance Computing for Multi-scale and Multi-physics Phenomena" from the Japan Science and Technology Agency.

Appendix A. Molecular force field functional forms and their combination rules

A.1. Adsorbate–adsorbate interactions

It is true that a number of homonuclear diatomic molecules as O_2 and N_2 molecules continue to be a theoretically important target to check the accuracy of elaborate ES theories [50–54,86–88]. However, they have also been studied because they show a variety of interesting characteristics in their solid states, e.g., α–β phase transition of solid O_2 [33–41]. There have been a large number of theoretical studies with respect to their molecular solid structures [36–44]. In particular, not only the electronic description of an isolated molecule itself but also the intermolecular interaction in the dimer is one of the principal interests since the latter is the main origin of their condensation. Similarly, the vdW small molecule dimers have been studied for a long time [36] as the smallest typical unit from a molecular solid, even though it lacks the collective properties.

Taking these circumstances into consideration, for the adsorbate–adsorbate interaction $V_{O_2\text{–}O_2}(\boldsymbol{R})$ between two O_2 molecules, its functional form was assumed to consist of a sum of a vdW part $V_{vdW}(\boldsymbol{R})$ and an EST one $V_{EQQ}(\boldsymbol{R})$ [36(b),39–41,47] as

$$V_{O_2\text{–}O_2}(\boldsymbol{R}) = V_{vdW}(\boldsymbol{R}) + V_{EQQ}(\boldsymbol{R}) \tag{A.1}$$

$$V_{vdW}(\boldsymbol{R}) = \sum_{i=1}^{2}\sum_{j=4}^{5} V_{LJ}(R_{ij}),$$

$$V_{EQQ}(\boldsymbol{R}) = \sum_{i=1}^{3}\sum_{j=4}^{6} \frac{q_i q_j}{4\pi\varepsilon_0 R_{ij}} \tag{A.2}$$

where the sum extends over both appropriate atoms and interaction sites on different molecules separated by the distances $R_{ij} \in \{R_{14}, R_{15}, R_{16}, R_{24}, R_{25}, R_{26}, R_{34}, R_{35}, R_{36}\} \equiv \boldsymbol{R}$ (Fig. A1). $V_{LJ}(R_{ij})$ is the effective Lennard–Jones (LJ) 12-6 potential function per pair of oxygen atoms [37,39,47], defined as

$$V_{LJ}(R_{ij}) = D_{O\text{–}O}\left[\left(\frac{R^e_{O\text{–}O}}{R_{ij}}\right)^{12} - 2\left(\frac{R^e_{O\text{–}O}}{R_{ij}}\right)^{6}\right] \tag{A.3}$$

where $D_{O\text{–}O}$ and $R^e_{O\text{–}O}$ are the effective well depth and the effective vdW distance between any two O atoms each belonging to a different O_2 molecule of the two, respectively [14,39,47].

In addition, $V_{EQQ}(\boldsymbol{R})$ was expressed approximately by placing three effective point charges $(q_O, q_X, q_O) = (-q, 2q, -q)$ along the molecular axis at $(z_0, 0, -z_0)$, respectively [39,40], with respect to the mass center, so that they might reproduce the electric quadrupole (Q) moment $Q = Q_{zz} - Q_{yy}$ [41,42,89]. The EQQ potential $V_{EQQ}(\boldsymbol{R})$ between two O_2 molecules is thus expressed by a combination of Coulombic interactions between each three charges on two different O_2 molecules.

Taking into consideration the orientation of O_2 molecules in the XRPD structure of CpPy·2O_2 [7], the parameters $D_{O\text{–}O}$ and $R^e_{O\text{–}O}$ were calibrated according to the *ab initio* ES calculations obtained recently by Bussery-Honvault et al. [32], i.e., *ab initio* ES calculations of the excited states of the O_2 dimer, corrected for basis set superposition errors (BSSE) and evaluated in a size consistent way. Surprisingly good agreement in the potential behavior was observed (cf. Table IV in Ref. [32]).

In Fig. A2(a), $V_{LJ}(R_{O\text{–}O})$ is shown, i.e., the presently optimized effective LJ 12-6 potential function between two oxygen atoms in an O_2 dimer. A set of parameters $D_{O\text{–}O}$ and $R^e_{O\text{–}O}$ for $V_{LJ}(R_{O\text{–}O})$ and q_O for $V_{EQQ}(R_{O\text{–}O})$ were obtained as 59.48 K (=0.1182 kcal/mol), 5.994 a_0 (=3.172 Å) and $-0.2227e$, respectively. $D_{O\text{–}O}$ and $R^e_{O\text{–}O}$ correspond to 1.280×10^{11} K a_0^{12}

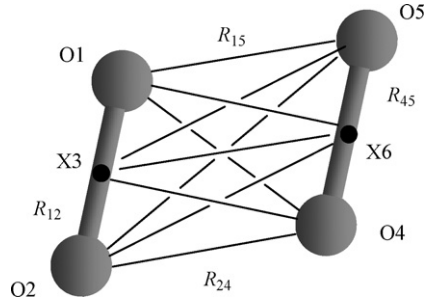

Fig. A1. Relative distances R between oxygen atoms and interaction points in an O_2 dimer.

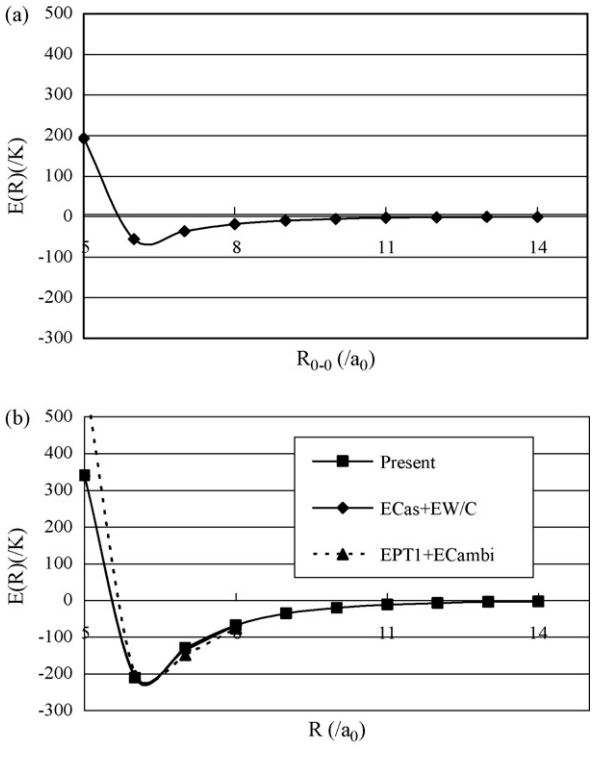

Fig. A2. (a) Effective LJ potential function between two oxygen atoms in an O_2 dimer and (b) total potential energy of the H-shaped O_2 dimer (X^1Ag).

and 2.759×10^6 K a_0^6 for so-called LJ parameters $A_{O\text{–}O}(= D_{O\text{–}O} R_{O\text{–}O}^{e12})$ and $B_{O\text{–}O}(= D_{O\text{–}O} R_{O\text{–}O}^{e6})$, fitted with their 95.00% confidence (the intervals of regression coefficients, 1.50×10^{10} K a_0^{12}, 7.17×10^5 K a_0^6 and $0.138e$, respectively). The value of the effective point charge $q_O = -0.2227e$, is reasonably in good agreement with the value $-0.2518e$ obtained by *ab initio* MO calculation at the UMP2/6-31+G(d)//UMP2/6-31+G(d) level of theory [70], where the ES-optimized interatomic distance R is 1.2463 Å (=$2z_0$) and the electric Q moment $Q = Q_{zz} - Q_{yy}$ results in -0.1956 DÅ that is naturally in good agreement with the MM-calculated value -0.1633 DÅ for the experimental interatomic distance 1.2110 Å (cf. the experimental Q, -0.39 DÅ [89]).

In Fig. A2(b), the total vdW potential for the H-shaped O_2 dimer (X^1Ag) is drawn, using $V_{LJ}(R_{O\text{–}O})$, as a function of the interatomic distance R between the centers of mass of two O_2 molecules. The present potential curve (■) is in very good agreement with those (♦ and ▲) that were obtained previously by a series of elaborate *ab initio* ES calculations [32]. The present values of D_{OO} and R_{OO}^e were very much in contrast to 0.060 kcal/mol and 3.929 Å in the universal force field (UFF) [90] or 3.9 Å in Hirschfelder et al. [91]. However, those were almost comparable to 54.34 K and 3.423 Å which were originally proposed by Pan et al. [47(b)] for the study of O_2 adsorption on graphite [48].

A.2. Intra-framework interaction and adsorbate–framework interaction

The intra-framework interaction for V_{CpPy} was also assumed as a sum of LJ and Coulomb potentials between constituent atoms of CpPy. Further, as is often conveniently adopted, the present framework–adsorbate interaction V_{CpPy-O_2} was constructed from the homonuclear (or diagonal) parameters through the use of an arithmetic mean combination rule for the LJ distance of a heteronuclear pair:

$$x_{IJ} = \tfrac{1}{2}(x_I + x_J) \tag{A.4}$$

where x_I is the atomic vdW distance of the Ith atom and the standard geometric combination rules for the well depth:

$$D_{IJ} = (D_I D_J)^{1/2} \tag{A.5}$$

where D_I is the atomic vdW energy of the Ith atom [13,14]. Values of the homonuclear parameters for the framework atoms are obtained from the universal force field (UFF) 1.02 [90], where, in general, bond lengths are correct usually to within 0.02 Å and bond angles usually to within 3° for a variety of organic molecules [90]. For an example, in a pyrazine molecule, it was reported that the C–C bond length is correctly calculated and the C–N bond is just 0.02 Å too long, although the C–N–C angle is overestimated by almost 5° [90].

EST interactions were calculated in kcal/mol by the following Coulombic form:

$$V_{EST}(R_{ij}) = G\left(\frac{q_i q_j}{\varepsilon R_{ij}}\right) \tag{A.6}$$

where q_i and q_j are the partial atomic point charges in electron units, and G is a constant 332.0637 so that the distance R_{ij} is in Å and ε is the dielectric constant 1.0 presently. Partial charges for the framework atoms were obtained using the QEq charge equilibration scheme [92], which, in general, leads to charges in excellent agreement with experimental dipole moments and with the atomic charges obtained from the EST potentials of accurate *ab initio* ES calculations [92].

Appendix B. Grand canonical Monte Carlo simulation and numerical parameters

The thermodynamic average $\langle A \rangle$ of an observable A, specifically the adsorbate molecules in the grand canonical (GC) ensemble, can be obtained by evaluating the following formula:

$$\langle A \rangle = Z^{-1} \sum_{N=0} \frac{a^N}{N!} \int_\Omega A(x^N) \exp\left(-\frac{V(x^N)}{k_B T}\right) \mathrm{d}x^N \tag{B.1}$$

where Z is the GC partition function defined as

$$Z = \sum_{N=0} \frac{a^N}{N!} \int_\Omega \exp\left(-\frac{V(x^N)}{k_B T}\right) \mathrm{d}x^N, \tag{B.2}$$

$$a = \left(\frac{h^2}{2\pi m k_B T}\right)^{-3/2} \lambda, \tag{B.3}$$

$$\lambda = \exp\left(\frac{\mu}{k_B T}\right). \tag{B.4}$$

The probability of a configuration $x^{N\pm1}$ in the GC ensemble can be obtained as

$$P(x^{N\pm1}) = Z^{-1}\left[\frac{a^{N\pm1}}{(N\pm1)!}\right] \exp\left(-\frac{V(x^{N\pm1})}{k_B T}\right). \tag{B.5}$$

In the Metropolis MC algorithm [15–17,93], the probability of realization accepting the random move, $x^N \to x^{N'}$, is chosen to be

$$W(x^N, x^{N'}) = \min\left[1; \frac{P(x^{N'})}{P(x^N)}\right], \tag{B.6}$$

where an adsorbate molecule in the framework is chosen at random and a rotation axis as well, and the molecule is translated by a random amount within a cube of size 2δ or rotated within the range $-\theta$ to $+\theta$, where δ and θ are the maximum step sizes whose values are typically 1.0 Å for the maximum translation step and 50.0° for the maximum rotation, respectively. In each simulation, 8M runs were executed, initial 1M runs were for equilibration and then not used for averaging [21].

References

[1] O.M. Yaghi, M. O'Keeffe, N.W. Ockwig, H.K. Chae, M. Eddaoudi, J. Kim, Nature 423 (2003) 705.
[2] (a) S. Kitagawa, R. Kitaura, S. Noro, Angew. Chem. 116 (2004) 2388; (b) S. Kitagawa, R. Kitaura, S. Noro, Angew. Chem. Int. Ed. 43 (2004) 2334.
[3] (a) S. Noro, S. Kitagawa, M. Kondo, K. Seki, Angew. Chem. 112 (2000) 2161;

S. Noro, S. Kitagawa, M. Kondo, K. Seki, Angew. Chem. Int. Ed. 39 (2000) 2082;
(b) K. Seki, W. Mori, J. Phys. Chem. B 106 (2002) 1380;
(c) G. Férey, M. Latroche, C. Serre, F. Millange, T. Loiseau, A. Percheron-Guégan, Chem. Commun. 24 (2003) 2976;
(d) D.N. Dybtsev, H. Chun, S.H. Yoon, D. Kim, K. Kim, J. Am. Chem. Soc. 126 (2004) 32;
(e) J.L.C. Rowsell, A.R. Millward, K.S. Park, O.M. Yaghi, J. Am. Chem. Soc. 126 (2004) 5666.
[4] R. Matsuda, R. Kitaura, S. Kitagawa, Y. Kubota, R.V. Belosludov, T.C. Kobayashi, H. Sakamoto, T. Chiba, M. Takata, Y. Kawazoe, Y. Mita, Nature 436 (2005) 238.
[5] (a) O. Ohmori, M. Fujita, Chem. Commun. (2004) 1586;
(b) J.S. Seo, D. Whang, H. Lee, S.I. Jun, J. Oh, Y.J. Jeon, K. Kim, Nature 404 (2000) 982.
[6] (a) M. Kondo, T. Okubo, A. Asami, S. Noro, T. Yoshitomi, S. Kitagawa, T. Ishii, H. Matsuzaka, K. Seki, Angew. Chem. 111 (1999) 190;
(b) M. Kondo, T. Okubo, A. Asami, S. Noro, T. Yoshitomi, S. Kitagawa, T. Ishii, H. Matsuzaka, K. Seki, Angew. Chem. Int. Ed. 38 (1999) 140.
[7] (a) R. Kitaura, S. Kitagawa, Y. Kubota, T.C. Kobayashi, K. Kindo, Y. Mita, A. Matsuo, M. Kobayashi, H.-C. Chang, T.C. Ozawa, M. Suzuki, M. Sataka, M. Takata, Science 298 (2002) 2358;
(b) T.C. Kobayashi, A. Matsuo, M. Suzuki, K. Kindo, R. Kitaura, R. Matsuda, S. Kitagawa, Prog. Theor. Phys. Suppl. 159 (2005) 271.
[8] D.E. Ellis, O. Warschkow, Coordin. Chem. Rev. 238–239 (2003) 31.
[9] (a) E.E. Santiso, K.E. Gubbins, Mol. Simul. 30 (2004) 699;
(b) F. Jensen, Introduction to Computational Chemistry, John Wiley & Sons, New York, 1999;
(c) P. von R. Schleyer (Ed.), Encyclopedia of Computational Chemistry, John Wiley & Sons, New York, 1998.
[10] (a) J. Simons, J. Phys. Chem. 95 (1991) 1017;
(b) J. Simons, An Introduction to Theoretical Chemistry, Cambridge University Press, Cambridge, 2003;
(c) E. Lewars, Computational Chemistry, Kluwer Academic Publishers, New York, 2003.
[11] (a) W.J. Hehre, L. Radom, P. von R. Schleyer, J.A. Pople, Ab Initio Molecular Orbital Theory, Wiley-Interscience Publication, New York, 1986;
(b) R.M. Martin, Electronic Structure Basic Theory and Practical Methods, Cambridge University Press, Cambridge, 2004.
[12] (a) U. Burkert, N.L. Allinger, Molecular Mechanics, ACS Monograph, vol. 177, ACS, Washington, 1982;
(b) A.K. Rappé, C.J. Casewit, Molecular Mechanics Across Chemistry, University Science Books, California, 1997.
[13] (a) M.P. Allen, D.J. Tildesley, Computer Simulation of Liquids, Clarendon, Oxford, 1987;
(b) A. Warshel, Computer Modeling of Chemical Reactions in Enzymes and Solutions, Wiley-Interscience Publication, New York, 1991.
[14] G.C. Maitland, M. Rigby, E.B. Smith, Q.A. Wakeham, Intermolecular Forces, Clarendon, Oxford, 1987.
[15] D.W. Heermann, Computer Simulation Methods, Springer, Berlin, 1990.
[16] D. Frenkel, B. Smit, Understanding Molecular Simulations, Academic Press, New York, 1996.
[17] (a) B. Smit, J.I. Siepmann, Science 264 (1994) 1118;
(b) B. Smit, J.I. Siepmann, J. Phys. Chem. 98 (1994) 8442;
(c) M.E. van Leeuwen, B. Smit, J. Phys. Chem. 99 (1995) 1831.
[18] (a) S.J. Goodbody, K. Watanabe, D. MacGowan, J.P.R.B. Walton, M. Quirke, J. Chem. Soc., Faraday Trans. 87 (1991) 1951;
(b) K. Watanabe, N. Austin, M.R. Stapleton, Mol. Simul. 15 (1995) 197;
(c) A.J. Richards, K. Watanabe, N. Austin, M.R. Stapleton, J. Porus Mater. 2 (1995) 43.
[19] Y. Ohta, H. Hitomi, M. Nagaoka, R. Matsuda, S. Kitagawa, Chem. Phys. Lett., submitted for publication.
[20] H. Hitomi, Y. Ohta, M. Nagaoka, R. Matsuda, S. Kitagawa, J. Am. Chem. Soc., submitted for publication.
[21] H. Hitomi, Y. Ohta, M. Nagaoka, R. Matsuda, S. Kitagawa, J. Phys. Chem. B, submitted for publication.
[22] (a) A. Nakamura, N. Ueyama, K. Yamaguchi (Eds.), Organometallic Conjugation, Springer, Berlin, 2002;
(b) T. Kawakami, S. Takamizawa, Y. Kitagawa, T. Maruta, W. Mori, K. Yamaguchi, Polyhedron 20 (2001) 1197.
[23] T. Sagara, J. Klassen, E. Ganz, J. Chem. Phys. 121 (2004) 12543.
[24] T. Sagara, J. Klassen, J. Ortony, E. Ganz, J. Chem. Phys. 123 (2005) 014701.
[25] G. Garberoglio, A.I. Skoulidas, J.K. Johnson, J. Phys. Chem. B 109 (2005) 13094.
[26] A.I. Skoulidas, D.S. Sholl, J. Phys. Chem. B 109 (2005) 15760.
[27] Q. Yang, C. Zhong, J. Phys. Chem. B 109 (2005) 11862.
[28] Q. Yang, C. Zhong, J. Phys. Chem. B 110 (2006) 655.
[29] Y. Kubota, M. Takata, R. Matsuda, R. Kitaura, S. Kitagawa, T.C. Kobayashi, Angew. Chem. Int. Ed. 45 (2006) 4932.
[30] R. Cambi, D. Cappelletti, G. Liuti, F. Pirani, J. Chem. Phys. 95 (1991) 1852.
[31] R. Hemández, R. Toumi, D.C. Clary, J. Chem. Phys. 102 (1995) 9544.
[32] (a) B. Bussery-Honvault, V. Veyret, J. Chem. Phys. 108 (1998) 3243;
(b) A. Campargue, L. Biennier, A. Kachanov, R. Jost, B. Bussery-Honvault, V. Veyret, S. Churassy, R. Bacis, Chem. Phys. Lett. 288 (1998) 734.
[33] M.F. Collins, Proc. Phys. Soc. 89 (1966) 415.
[34] C.S. Barrett, L. Meyer, I. Wasserman, J. Chem. Phys. 47 (1967) 592.
[35] E.J. Wachtel, R.G. Wheeler, J. Appl. Phys. 42 (1971) 1581.
[36] (a) C.A. English, J.A. Venables, Proc. Roy. Soc. Lond. A 340 (1974) 57;
(b) C.A. English, J.A. Venables, D.R. Salahub, Proc. Roy. Soc. Lond. A 340 (1974) 81.
[37] M.L. Klein, D. Levesque, J.-J. Weis, Phys. Rev. B 21 (1980) 5785.
[38] G.C. DeFotis, Phys. Rev. B 23 (1981) 4715.
[39] R.D. Etters, A.A. Helmy, K. Kobashi, Phys. Rev. B 28 (1983) 2167.
[40] (a) A.A. Helmy, K. Kobashi, R.D. Etters, J. Chem. Phys. 80 (1984) 2782;
(b) A.A. Helmy, K. Kobashi, R.D. Etters, J. Chem. Phys. 82 (1985) 4731.
[41] R.D. Etters, K. Kobashi, J. Belak, Phys. Rev. B 32 (1985) 4097.
[42] C. Uyeda, K. Sugiyama, M. Date, J. Phys. Soc. Jpn. 54 (1985) 1107.
[43] A.P.J. Jansen, A van der Avoird, J. Chem. Phys. 86 (1987) 3583.
[44] K. Nozawa, N. Shima, K. Makoshi, J. Phys. Soc. Jpn. 71 (2002) 377.
[45] W.A. Steele, Surf. Sci. 36 (1973) 317.
[46] M. Nielsen, J.P. McTague, Phys. Rev. B 19 (1979) 3096.
[47] (a) R.D. Etters, R.-P. Pan, V. Chandrasekharan, Phys. Rev. Lett. 45 (1980) 645;
(b) R.-P. Pan, R.D. Etters, K. Kobashi, V. Chandrasekharan, J. Chem. Phys. 77 (1982) 1035.
[48] Y.P. Joshi, D.J. Tildesley, Surf. Sci. 166 (1986) 169.
[49] S.Y. Tang, W. Jin, S.D. Mahanti, R.K. Kalia, Phys. Rev. B 39 (1989) 677.
[50] M.C. van Hemert, P.E.S. Wormer, A. van der Avoird, Phys. Rev. Lett. 51 (1983) 1167.
[51] P.E.S. Wormer, A. van der Avoird, J. Chem. Phys. 81 (1984) 1929.
[52] B. Bussery, P.E.S. Wormer, J. Chem. Phys. 99 (1993) 1230.
[53] B. Bussery, S.Ya. Umanskii, M. Aubert-Frécon, O. Bouty, J. Chem. Phys. 101 (1994) 416.
[54] H. Hettema, P.E.S. Wormer, P. Jorgensen, H.J.A. Jensen, T. Helgaker, J. Chem. Phys. 101 (1994) 1297.
[55] P. Demontis, G.B. Suffritti, Chem. Rev. 97 (1997) 2845.
[56] (a) G.M. Day, W.D.S. Motherwell, H.L. Ammon, S.X.M. Boerrigter, R.G. Della Valle, E. Venuti, A. Dzyabchenko, J.D. Dunitz, B. Schweizer, B.P. van Eijck, P. Erk, J.C. Facelli, V.E. Bazterra, M.B. Ferraro, D.W.M. Hofmann, F.J.J. Leusen, C. Liangm, C.C. Pantelides, P.G. Karamertzanis, S.L. Price, T.C. Lewis, H. Nowell, A. Torrisi, H.A. Scheraga, Y.A. Arnautova, M.U. Schmidtk, P. Verwer, Acta Crystallogr. B 61 (2005) 511;
(b) H. Nowell, S.L. Price, Acta Crystallogr. B 61 (2005) 558.
[57] J.-R. Hill, A.R. Minihan, E. Wimmer, C.J. Adams, Phys. Chem. Chem. Phys. 2 (2000) 4255.
[58] D.A. Faux, J. Phys. Chem. B 103 (1999) 7803.
[59] P. Hohenberg, W. Kohn, Phys. Rev. B 136 (1964) 864.
[60] W. Kohn, L.J. Sham, Phys. Rev. A 140 (1965) 1133.
[61] M.C. Payne, M.P. Teter, D.C. Allan, T.A. Arias, J.D. Joannopoulos, Rev. Mod. Phys. 64 (1992) 1045.
[62] M.D. Segall, P.J.D. Lindan, M.J. Probert, C.J. Pickard, P.J. Hasnip, S.J. Clark, M.C. Payne, J. Phys. Condens. Mat. 14 (2002) 2717.
[63] D.M. Ceperley, B.I. Alder, Phys. Rev. Lett. 45 (1980) 566.
[64] J.P. Perdew, A. Zunger, Phys. Rev. B 23 (1981) 5048.

[65] D. Vanderbilt, Phys. Rev. B 41 (1990) 7892.
[66] H.J. Mokhorst, J.D. Pack, Phys. Rev. B 13 (1990) 7892.
[67] (a) Material Studio CASTEP Accelrys Inc., San Diego, 2001;
(b) V. Milman, B. Winkler, J.A. White, C.J. Pickard, M.C. Payne, E.V. Akhmatskaya, R.H. Nobes, Int. J. Quant. Chem. 77 (2000) 895.
[68] C. Lee, W. Yang, R.G. Parr, Phys. Rev. B 37 (1990) 385.
[69] A.D. Becke, J. Chem. Phys. 98 (1993) 5648.
[70] (a) C. Møller, M.S. Plesset, Phys. Rev. 46 (1934) 618;
(b) L. Brillouin, Actualities Soc. Ind. 71 (1934) 159;
(c) J.A. Pople, R. Seeger, R. Krishnan, Int. J. Quant. Chem. Symp. 11 (1977) 149.
[71] M.J. Frisch, et al., Gaussian03, Revision B.03, Gaussian Inc., Pittsburgh, PA, 2003.
[72] For example:
(a) K. Grzelakowski, I. Lyuksyutov, E. Bauer, Phys. Rev. B 45 (1992) 6877;
(b) K. Thürmer, C.B. Carter, N.C. Bartelt, R.Q. Hwang, Phys. Rev. Lett. 92 (2004) 106101.
[73] (a) R. Car, M. Parrinello, Phys. Rev. Lett. 55 (1985) 2471;
(b) M. Parrinello, Solid State Commun. 102 (1997) 107.
[74] D. Marx, J. Hutter, in: J. Grotendorst (Ed.), Modern Methods and Algorithms of Quantum Chemistry Proceedings (NIC Series Vol. 1), John von Neumann-Institute for Computing, Jülich, 2000, p. 329.
[75] Material Studio Accelrys Inc., San Diego, 2001.
[76] (a) F. Darkrim, D. Levesque, J. Chem. Phys. 109 (1998) 4981;
(b) F. Darkrim, D. Levesque, J. Chem. Phys. 104 (2000) 6773.
[77] J.E. Straub, M. Karplus, Chem. Phys. 158 (1991) 221.
[78] B.J. Berne, G.D. Harp, Adv. Chem. Phys. 18 (1970) 63.
[79] T. Uemura, K. Kitagawa, S. Horike, T. Kawamura, S. Kitagawa, M. Mizuno, K. Endo, Chem. Commun. (2006) 5968.
[80] (a) T. Uemura, R. Kitaura, Y. Ohta, M. Nagaoka, S. Kitagawa, Angew. Chem. 118 (2006) 4218;
(b) T. Uemura, R. Kitaura, Y. Ohta, M. Nagaoka, S. Kitagawa, Angew. Chem. Int. Ed. 45 (2006) 4112.
[81] M. Takayanagi, H. Okumura, M. Nagaoka, J. Phys. Chem. B 111 (2007) 864.
[82] J. Kärger, D.M. Ruthven, Diffusion in Zeolites and Other Microporous Solids, Wiley Interscience Publisher, New York, 1992.
[83] H. Tanaka, H. Kanoh, M. Yudasaka, S. Iijima, K. Kaneko, J. Am. Chem. Soc. 127 (2005) 7511.
[84] K. Uemura, K. Saito, S. Kitagawa, H. Kita, J. Am. Chem. Soc. 128 (2006) 16122.
[85] K. Saito, P-020: Proceedings of Second International Symposium on Chemistry of Coordination Space (ISCCS 2006), Fukuoka, Japan, 2006.
[86] L. Bytauats, K. Ruedenberg, J. Chem. Phys. 122 (2005) 154110.
[87] R.M. Berms, A. van der Avoird, J. Chem. Phys. 72 (1980) 6107.
[88] J. Tennyson, A. van der Avoird, J. Chem. Phys. 77 (1982) 5664.
[89] D.E. Strogyn, A.P. Strogyn, Mol. Phys. 11 (1966) 371.
[90] (a) A.K. Rappé, C.J. Casewit, K.S. Colwell, W.A. Goddard III, W.M. Skiff, J. Am. Chem. Soc. 114 (1992) 10024;
(b) C.J. Casewit, K.S. Colwell, A.K. Rappé, J. Am. Chem. Soc. 114 (1992) 10035;
(c) C.J. Casewit, K.S. Colwell, A.K. Rappé, J. Am. Chem. Soc. 114 (1992) 10046.
[91] J.O. Hirschfelder, C.F. Curtiss, R.B. Bird, Molecular Theory of Gases and Liquids, Wiley, New York, 1954.
[92] A.K. Rappé, W.A. Goddard III, J. Phys. Chem. 95 (1991) 3358.
[93] N. Metropolis, A.W. Rosenbluth, M.N. Rosenbluth, A.H. Teller, E. Teller, J. Chem. Phys. 21 (1953) 1087.